Author's personal copy

Provided for non-commercial research and educational use only.
Not for reproduction, distribution or commercial use.

This article was originally published in the book *Encyclopedia of Atmospheric Sciences*, 2nd edition. The copy attached is provided by Elsevier for the author's benefit and for the benefit of the author's institution, for non-commercial research, and educational use. This includes without limitation use in instruction at your institution, distribution to specific colleagues, and providing a copy to your institution's administrator.

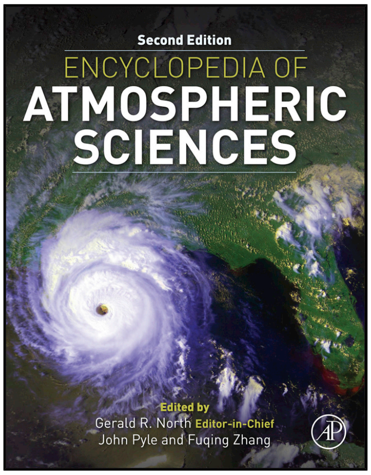

All other uses, reproduction and distribution, including without limitation commercial reprints, selling or licensing copies or access, or posting on open internet sites, your personal or institution's website or repository, are prohibited. For exceptions, permission may be sought for such use through Elsevier's permissions site at:
http://www.elsevier.com/locate/permissionusematerial

From Durran, D.R., 2015. Lee Waves and Mountain Waves. In: Gerald R. North (editor-in-chief), John Pyle and Fuqing Zhang (editors). Encyclopedia of Atmospheric Sciences, 2nd edition, Vol 4, pp. 95–102.
ISBN: 9780123822253
Copyright © 2015 Elsevier Ltd. unless otherwise stated. All rights reserved.
Academic Press

Lee Waves and Mountain Waves

DR Durran, University of Washington, Seattle, WA, USA

© 2015 Elsevier Ltd. All rights reserved.

Synopsis

The basic properties of mountain waves are discussed using linear theory for small-amplitude disturbances. Important nonlinear processes governing waves launched by larger mountains are then considered. The final topic is mountain-wave momentum flux and the interaction of these waves with the larger-scale flow.

Introduction

Buoyancy perturbations develop when stably stratified air ascends a mountain barrier. These perturbations often trigger disturbances that propagate away from the mountain as gravity (or buoyancy) waves. Gravity waves triggered by the flow over a mountain are referred to as 'mountain waves' or 'lee waves.' Mountain waves sometimes reveal their presence through dramatic cloud formations, such as smooth lenticular clouds (see Figures 1 and 2) and ragged rotor clouds. Large-amplitude mountain waves can generate regions of clear air turbulence that pose a hazard to aviation. Large-amplitude mountain waves may also produce very strong winds that blow down the lee slope of ridgelike topographic barriers (*see* **Mountain Meteorology:** Downslope Winds).

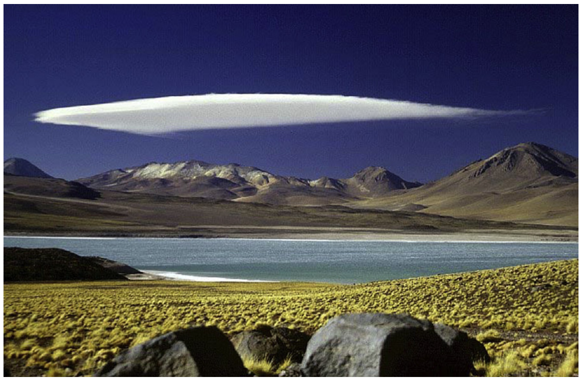

Figure 1 Single lenticular cloud over Laguna Verde, Bolivia. This cloud was probably formed by a vertically propagating mountain wave. Copyright Bernhard Mühr, www.wolkenatlas.de.

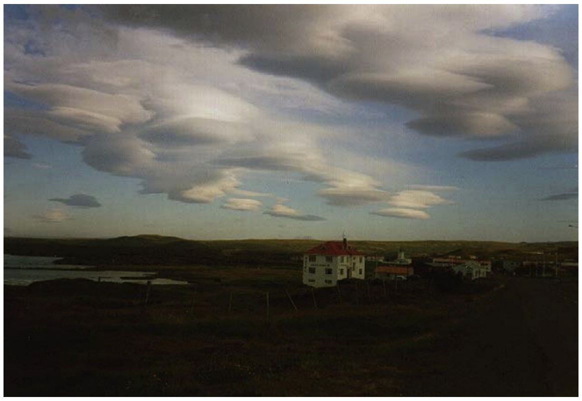

Figure 2 Multiple lenticular clouds over Mývatin, Iceland, formed by trapped lee waves. Copyright Georg Müller, www.wolkenatlas.de.

What happens to mountain waves after they are generated? If the wave amplitude becomes large in comparison to the vertical wavelength, the streamlines in a vertically propagating mountain wave steepen and overturn in a manner roughly analogous to a breaking wave in the ocean. Such 'convective' overturning often occurs as the waves enter the lower stratosphere where they encounter increased static stability and decreasing horizontal wind speeds. The convective overturning of vertically propagating waves is also promoted by the systematic decrease in atmospheric density with height. Those waves that do not breakdown due to convective overturning before reaching the mesosphere are ultimately dissipated by the vertical transfer of infrared radiation between the warm and cool regions within the wave and the surrounding atmosphere (radiative damping).

Horizontal momentum is transported by mountain waves from the regions of wave dissipation to the surface where a net pressure force is exerted on the topography. A decelerative force is exerted on the large-scale atmospheric circulation in those regions where the wave undergoes dissipation.

The basic structure of a mountain wave is determined by the size and shape of the mountain and by the vertical profiles of temperature, wind speed, and moisture in the impinging flow. The overall character of the wave can often be predicted on the basis of linear theory, in which the mountain is assumed to be small in comparison with the vertical wavelength of the mountain wave, and such theory will be the subject of the next section. Nevertheless, nonlinear effects do exert a significant influence on the wave amplitude and are essential to the dynamics of mountain-wave dissipation in regions of wave breaking; such effects will be considered later in this article.

Linear Mountain-Wave Theory

The strongest mountain waves are forced by long quasi-two-dimensional ridges that are sufficiently narrow so that the dynamical influence of the Coriolis force can be neglected. The

Encyclopedia of Atmospheric Sciences, Second Edition, 2015, 95–102

basic dynamics of these waves are largely captured by the linear theory for steady two-dimensional Boussinesq flow over an obstacle, for which the linearized momentum, thermodynamic, and continuity equations may be reduced to the following single equation for the vertical velocity w,

$$\frac{\partial^2 w}{\partial x^2} + \frac{\partial^2 w}{\partial z^2} + \ell^2 w = 0. \qquad [1]$$

Here x is the horizontal coordinate perpendicular to the ridge-line; z is the vertical coordinate, and

$$\ell^2 = \frac{N^2}{U^2} - \frac{1}{U}\frac{\mathrm{d}^2 U}{\mathrm{d}z^2} \qquad [2]$$

is the 'Scorer parameter' in which $U(z)$ is the speed of the basic-state flow and $N(z)$ is the Brunt-Väisälä frequency (or alternatively, the buoyancy frequency). In the Boussinesq limit, the Brunt-Väisälä frequency may be defined in terms of the basic-state potential temperature $\overline{\theta}(z)$, a constant reference potential temperature θ_0, and the gravitational acceleration g, such that $N^2 = (g/\theta_0)\mathrm{d}\overline{\theta}/\mathrm{d}z$.

Neglecting the effects of surface friction, the velocity perpendicular to the topography must vanish at the surface of the topography $z = h(x)$. This constraint provides a lower boundary condition for eqn [1], and can be approximated as $w(x,0) = U\partial h/\partial x$ to the same order of accuracy retained in the linearized governing equations. The atmosphere has no distinct upper boundary, so the upper boundary condition is imposed in the limit $z \rightarrow \infty$. In order to ensure the physical relevance of mathematical solutions to eqn [1] in the infinitely deep atmosphere, those solutions must satisfy one of the two possible conditions, that is, either (i) the perturbation energy density must approach zero as $z \rightarrow \infty$, or (ii) if the perturbation energy density is finite as $z \rightarrow \infty$, then the perturbation energy flux associated with each individual's vertically propagating mode must be upward. The second condition allows the representation of disturbances generated within the domain that propagate energy upward to arbitrarily great heights, but it prohibits downward propagating modes from radiating energy into the domain from infinity.

Constant Wind Speed and Stability, Sinusoidal Ridges

As a first example consider flow in a horizontally periodic domain in which $h(x) = h_0\sin(kx)$. The lower boundary condition becomes $w(x,0) = Uh_0k\cos kx$, and solutions to eqn [1] subject to this lower boundary condition may be written in the form

$$w(x,z) = \tilde{w}_1(z)\cos kx + \tilde{w}_2(z)\sin kx. \qquad [3]$$

Substituting eqn [3] into eqn [1], one obtains

$$\frac{\mathrm{d}^2\tilde{w}_i}{\mathrm{d}z^2} + \left(\ell^2 - k^2\right)\tilde{w}_i = 0 \quad i = 1,2. \qquad [4]$$

Consider the simplest possible atmospheric structure in which N and U are constant with height. Without loss of generality we will focus on the case in which $U > 0$ and $k > 0$. Since N and U are constant, $\ell^2 = N^2/U^2$ is also constant. Defining $\nu = (\ell^2 - k^2)^{1/2}$ and $\mu^2 = -\nu^2$, the solution to eqn [4] may be written as

$$\tilde{w}_i(z) = \begin{cases} A_i e^{\mu z} + B_i e^{-\mu z} & k > \ell, \\ C_i\cos\nu z + D_i\sin\nu z & k < \ell, \end{cases} \qquad [5]$$

where A, B, C, and D are constants to be determined by the upper and lower boundary conditions. Note that the fundamental character of the solution depends on the relative magnitudes of the Scorer parameter and the horizontal wavenumber.

If $\ell < k$, or equivalently, if the intrinsic frequency of the wave Uk is greater than N, solutions to eqn [4] either grow or decay exponentially with height. Only the solution that decays with height is admitted by the upper boundary condition that the perturbation energy density must approach zero as $z \rightarrow \infty$. The vertical velocity satisfying eqn [1] and the upper and lower boundary conditions is

$$w(x,z) = Uh_0ke^{-\mu z}\cos kx. \qquad [6]$$

On the other hand, if $\ell > k$, the solutions to eqn [4] are sinusoidal functions of z that neither amplify nor decay as $z \rightarrow \infty$. After imposing the lower boundary condition, the general solution can be expressed as

$$w(x,z) = (Uh_0k - E)\cos(kx + \nu z) + E\cos(kx - \nu z), \qquad [7]$$

where the constant E is determined by the upper boundary condition. Writing the solution in the form eqn [7] makes it easy to distinguish between waves that propagate energy upward or downward by examining the relationship between the signs of the vertical and horizontal wavenumbers.

The perturbation energy in a wave propagates at the group velocity. In the constant-N-and-U case, the dispersion relation for the time-dependent generalization of eqn [1] is

$$\omega = Uk \pm \frac{Nk}{(k^2 + \nu^2)^{1/2}}, \qquad [8]$$

where ω is the frequency and k and ν are the horizontal and vertical wavenumbers in an arbitrary wave of the form $\Re(e^{i(kx+\nu z-\omega t)})$. Since by assumption $U > 0$, all steady waves (for which $\omega = 0$) are associated with the negative root in eqn [8], and their vertical group velocities are

$$\frac{\partial\omega}{\partial\nu} = \frac{Nk\nu}{(k^2 + \nu^2)^{3/2}}, \qquad [9]$$

implying that upward group velocity, and upward energy transport, occurs when k and ν have the same sign. The upper boundary condition therefore requires $E = 0$ in eqn [7], and when $\ell > k$, the solution to eqn [1] becomes

$$w(x,z) = Uh_0k\cos(kx + \nu z). \qquad [10]$$

The difference between the case $\ell < k$ and the case $\ell > k$ is illustrated in **Figure 3**, which shows streamlines over a series of sinusoidal ridges in a steady flow with $N = 0.01\ \mathrm{s}^{-1}$ and $U = 15\ \mathrm{m\ s}^{-1}$. In the case shown in **Figure 3(a)**, the topographic wavelength is 8 km and $\ell^2 < k^2$ (or equivalently $Uk > N$); the waves decay exponentially with height, and the wave crests are aligned vertically. In the case in **Figure 3(b)**, the topographic wavelength is 40 km and $\ell^2 > k^2$ (or $Uk < N$); the waves propagate vertically without loss of amplitude, and the wave crests tilt upstream with height. The waves decay away from the forcing when the intrinsic frequency exceeds the

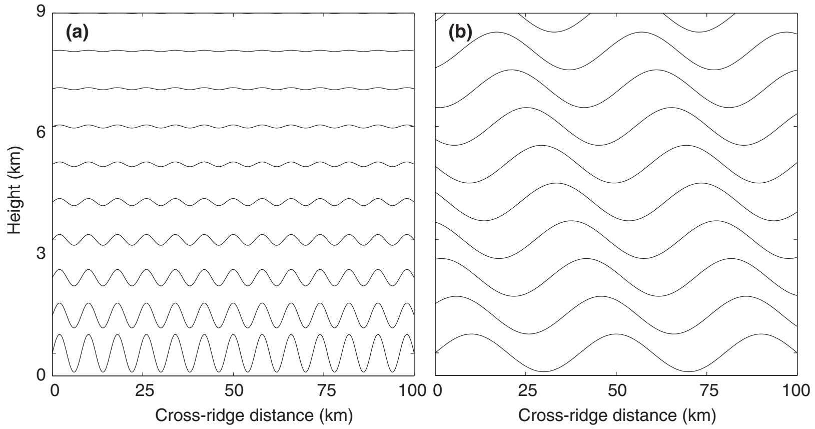

Figure 3 Streamlines in steady airflow over an infinite series of sinusoidal ridges when $N = 0.01\ \mathrm{s}^{-1}$, $U = 15\ \mathrm{m\ s}^{-1}$, and the wavelength of the topography is (a) 8 km (case $Uk > N$) or (b) 40 km (case $Uk < N$). The flow is from left to right. The lowest streamline coincides with the topography.

Brunt-Väisälä frequency ($Uk > N$) because there is no way for buoyancy restoring forces to support oscillations at such high frequencies (*see* **Gravity Waves:** Buoyancy and Buoyancy Waves: Optical Observations; Buoyancy and Buoyancy Waves: Theory). On the other hand, when the intrinsic frequency is less than the Brunt-Väisälä frequency, vertical propagation occurs because buoyancy restoring forces can support air-parcel oscillations along a path slanted off the vertical at an angle $\phi = \cos^{-1}(Uk/N)$. In steady mountain waves, ϕ is the angle at which lines of constant phase tilt off the vertical.

Isolated Mountain, Vertical Variations in *N* or *U*

The mountain-wave solutions [6] and [10] are only valid for air streams with constant basic-state wind speed and stability flowing across an endless series of sinusoidal ridges. If more realistic terrain profiles and atmospheric structures are considered, other linear solutions can be obtained that more strongly resemble observed mountain waves. In this section, we will describe how the wave response is influenced by isolated topography and vertical variations in atmospheric wind speed and stability.

Suppose that the mountain profile consists of a single ridge from which the terrain elevation drops to some reference level at all distances sufficiently far upstream and downstream. Just as Fourier series can be used to represent a wide variety of periodic functions with an infinite sum of sines and cosines, the isolated mountain can, under rather general conditions, be constructed from periodic functions by the use of Fourier transforms. Let $\widehat{w}(k,z)$ denote the Fourier transform of $w(x,z)$ with respect to the x-coordinate, and let $\widehat{h}(k)$ be the Fourier transform of the topography $h(x)$.

The k-th component of the Fourier transformed vertical velocity $\widehat{w}(k,z)$ must satisfy the Fourier transform of the governing eqn [1],

$$\frac{\partial^2 \widehat{w}}{\partial z^2} + \left(\ell^2 - k^2\right)\widehat{w} = 0, \qquad [11]$$

which has the same form as eqn [4]. The lower boundary condition transforms to $\widehat{w}(k,0) = iUkh_0\widehat{h}$. When N and U are constant, the solution to eqn [11], subject to the appropriate upper and lower boundary conditions, is

$$\widehat{w}(k,z) = ikU\widehat{h}(k)\exp\left[i\left(\ell^2 - k^2\right)^{1/2}z\right], \quad k > 0. \qquad [12]$$

Equation [12] is just the complex analog of eqn [5]; each Fourier component $\widehat{w}(k,z)$ of the transformed vertical velocity is identical to the $\tilde{w}_i$ forced by an infinite series of sinusoidal ridges having wavenumber k and amplitude $\widehat{h}(k)$. The solutions obtained in the preceding section are therefore also applicable to the case of isolated topography. The only complication arises from the requirement that after the $\widehat{w}(k,z)$ are determined, the total vertical velocity $w(x,z)$ must be obtained by computing an inverse Fourier transform. The relative weight attached to each individual wavenumber in the composite solution is determined by the Fourier transform of the mountain.

Streamlines for steady linear flow over an isolated ridge of the form

$$h(x) = \frac{h_0 a^2}{x^2 + a^2} \qquad [13]$$

are shown in **Figure 4(a)** for the case $N = 0.01047\ \mathrm{s}^{-1}$, $U = 10\ \mathrm{m\ s}^{-1}$, and $Nh_0/U = 0.6$.

In this case, $Na/U \approx 10$ and the dominant horizontal wavenumbers in the Fourier transform of the topography satisfy $k^2 \ll \ell^2$, which eliminates the dependence of the vertical structure on the horizontal wavenumber in eqn [12]. As a result, all modes associated with these dominant wavenumbers have approximately the same vertical wavelength ($2\pi U/N = 6$ km), so the streamline at 6 km approximately reproduces the mountain profile while those at 3 and 9 km are roughly the mirror-image of the topography. The solution shown in **Figure 4(a)** is computed numerically without making the hydrostatic assumption and is very similar to that which would be obtained in the hydrostatic limit, in which all horizontal wavenumbers have exactly the same vertical wavelength and the mountain profile is exactly reproduced by the streamline originating at the 6 km level upstream.

As suggested by **Figure 4(a)**, when an infinitely long ridge is sufficiently wide that the flow is approximately hydrostatic

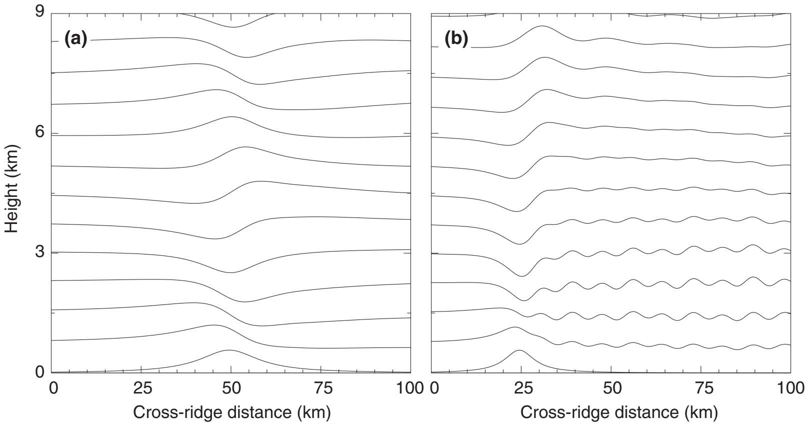

Figure 4 Streamlines in steady airflow over an isolated mountain as predicted by linear theory when (a) $a = 10$ km, N is constant, and $Nh_0/U = 0.6$; (b) $a = 5$ km, N is constant throughout each of two layers such that between the surface and 3 km $N_L h_0/U = 0.6$, and above 3 km $N_U h_0/U = 0.24$.

$(Na/U \gg 1)$ but still narrow enough that Coriolis forces can be neglected ($|f|a/U \ll 1$, where f is the Coriolis parameter), energetic mountain waves are found only in the region directly above the mountain. In the nonhydrostatic case, some waves do appear in the region downstream from the ridge, as can be deduced from the horizontal group velocity $\partial\omega/\partial k$, which using eqn [8] and again assuming $U > 0$, may be expressed as

$$\frac{\partial\omega}{\partial k} = \frac{\omega}{k} + \frac{Nk^2}{(k^2 + \nu^2)^{3/2}}. \qquad [14]$$

The first term in eqn [14] is the phase speed, which is zero for a steady mountain wave. The second term is nonnegative, implying downstream energy propagation – except in the hydrostatic limit when the second term vanishes because $k^2/\nu^2 \to 0$. A sufficient decrease in the width of the mountain, relative to that shown in **Figure 4(a)**, will therefore lead to the generation of nonhydrostatic waves that populate a wedge-shaped region emanating upward and downstream from the mountain. The wave energy for each component of the total solution propagates along a line whose slope is equal to the ratio of the vertical group velocity to the horizontal group velocity for that component. Quasi-uniform low-level wave trains, such as those shown in **Figure 4(b)**, do not however, occur unless there are significant vertical variations in the wind speed and static stability.

If the vertical variations in U and N are such that the Scorer parameter decreases significantly with height, cross-ridge flow may generate a qualitatively different type of wave, the 'trapped lee wave.' A series of trapped lee waves (also known as resonant lee waves) are apparent extending downstream from the ridge throughout the layer $0 \le z \le 4$ km in **Figure 4(b)**; a vertically propagating wave is also visible directly above the mountain. The streamlines shown in **Figure 4(b)** are for the linear solution to the same problem considered in **Figure 4(a)**, except that $a = 5$ km and the static stability above 3 km is reduced by a factor of 0.4. (The Brunt-Väisälä frequencies in the upper and lower layers are thus $N_U = 0.004188$ and $N_L = 0.01047$ s^{-1}, respectively.)

A necessary condition for the existence of trapped waves in the two-layer problem is that

$$\ell_L^2 - \ell_U^2 > \frac{\pi^2}{4H^2}, \qquad [15]$$

where ℓ_U and ℓ_L are the Scorer parameters in the upper and lower layers, and H is the depth of the lower layer. Equation [15] states that the difference in wave propagation characteristics in the two layers must exceed a certain threshold before the waves can be trapped. The horizontal wavenumber of any resonant lee wave in the two-layer system satisfies $\ell_L > k > \ell_U$, implying that the wave propagates vertically in the lower layer and decays exponentially with height in the upper layer. As shown in **Figure 4(b)**, trapped waves have no tilt, even though they can propagate vertically in the lower layer. The reason for this is that wave energy is repeatedly reflected, without loss of amplitude, from the upper layer and the flat ground downstream from the mountain. As a result, the downstream disturbance is the superposition of equal-amplitude upward and downward propagating waves, a combination which has no tilt.

Nonlinear Mountain Waves

Now suppose that the mountain height is not small compared to the vertical wavelength of the mountain wave. If N and U are constant, the streamline displacement $\delta(x,z)$ in steady two-dimensional Boussinesq flow over such a ridge is still governed by a relatively simple mathematical model known as Long's equation

$$\frac{\partial^2\delta}{\partial x^2} + \frac{\partial^2\delta}{\partial z^2} + \frac{N^2}{U^2}\delta = 0, \qquad [16]$$

Although Long's equation is a linear partial differential equation, it may be derived from the fully nonlinear equations without making any linearization or small-amplitude assumptions. Nevertheless, eqn [16] may also be derived by assuming the mountain is infinitesimally high and linearizing the

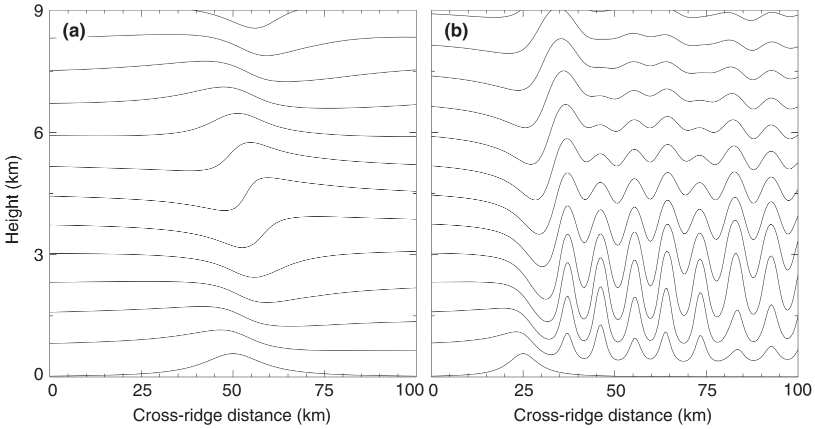

Figure 5 As in **Figure 2** except that the streamlines are for a fully nonlinear flow as computed using a numerical model. The trapped waves in panel b are not completely steady; the solution is shown a nondimensional time $Ut/a = 20$ after starting the flow from rest.

governing equations in the usual manner. When N and U are constant, the only difference between the linear and nonlinear solutions arises from the lower boundary condition, which requires $\delta[x,h(x)] = h(x)$ in the exact finite-amplitude case and is approximated by $\delta(x,0) = h(x)$ in the small-amplitude limit.

As one might guess from the similarities in the governing equations, when N and U are constant the influence of nonlinear dynamics on the wave structure is often relatively minor. This similarity can be appreciated by comparing the linear solution in **Figure 4(a)** with the corresponding nonlinear solution in **Figure 5(a)**, both of which show streamlines in a Boussinesq flow for which $Nh_0/U = 0.6$.

Nonlinear processes steepen the streamlines around $z = 4.5$ km, which is 3/4 of a vertical wavelength ($3\lambda_z/4$) above the topography. Conversely, the nonlinear waves are less steep than their linear counterparts near $z = 1.5$ km, which is $\lambda_z/4$ above the mean height of the topography. Despite these modest differences in the shape of the streamlines in the linear and nonlinear waves, the wave amplitude is almost identical in both cases. Nonlinear processes do not have a dramatic impact on the waves forced by flow over an infinitely long ridge unless either (i) there are vertical variations in N and U or (ii) the mountain is high enough to force wave overturning.

The influence of nonlinear wave dynamics on the flow in the two-layer atmosphere previously considered in connection with **Figure 4(b)** is shown in **Figure 5(b)**. The amplitude of the lee waves in the nonlinear solution is much larger than that in the linear solution, and in the nonlinear case significant variations are visible among the individual troughs and crests in the region $65 \leq x \leq 100$ km. As suggested by this example, and demonstrated in several observational campaigns and numerical studies, linear theory does reliably predict the amplitude of trapped lee waves generated by finite-amplitude mountains. The main shortcoming of linear theory is that it cannot capture the tendency of the nonlinear dynamics to enhance the short-wavelength Fourier components in the low-level wave field over the lee slope. The nonlinear enhancement of these short-wavelength perturbations in the first wave above the mountain often produces more forcing at the wavelength of the resonant lee waves than does the direct forcing by the topographic profile itself.

Clouds that form in regions of net upward displacement in vertically propagating hydrostatic waves may appear like the cloud in **Figure 1**. The large single region of cloudiness parallel to the mountain crest is probably formed by air-parcel displacements qualitatively similar to those in the streamline originating near the 6-km-level in **Figure 5(a)**.

Clouds that form in trapped lee waves may appear as a series of long bands parallel to the generating ridge. Such bands are often visible in satellite photos and are formed by streamline patterns qualitatively similar to those originating in the layer between 2 and 4 km in **Figure 5(b)**. Nevertheless, three dimensional variations in the upstream topography often break these bands into the superposition of many lens-shaped cloud masses, such those shown in **Figure 2**.

Returning to the discussion of how nonlinear dynamics modify the structure of mountain waves, consider the influence of wave breaking on the flow. Two examples in which the wave amplitude becomes large enough to overturn are shown in **Figure 6**.

The case shown in **Figure 6(a)** is one with constant N and U identical to that in **Figure 5(a)**, except that the mountain height is increased so that $Nh_0/U = 1.2$. (The vertical scale also extends to $z = 15$ km.) Wave overturning first begins at the $3\lambda_z/4$ level, which is the same level at which the wave faces appear to be steepened in **Figure 5(a)**. As the wave begins to overturn, a $\lambda_z/2$ deep region of well-mixed stagnant fluid develops over the lee slope and begins to extend downstream. A second region of wave overturning eventually develops at a height of $7\lambda_z/4$, although the perturbations are weaker at this level due to the dissipation experienced by the wave as it propagates through the first wave-breaking level. **Figure 6** shows the solution at a nondimensional time (Ut/a) of 30, by which time the near-mountain solution is quasi-steady, but the layers of well-mixed fluid in the wave-breaking region continue to expand further downstream. Also shown are contours of the subgrid-scale eddy diffusivity. Regions in which the subgrid-scale diffusivity is large are regions in which the numerical model has diagnosed the presence of vigorous small-scale turbulence such as that which occurs due to wave breaking.

Although the breaking of mountain waves in an atmosphere with constant N and U has received a great deal of theoretical attention, the morphology of such flows is not representative of

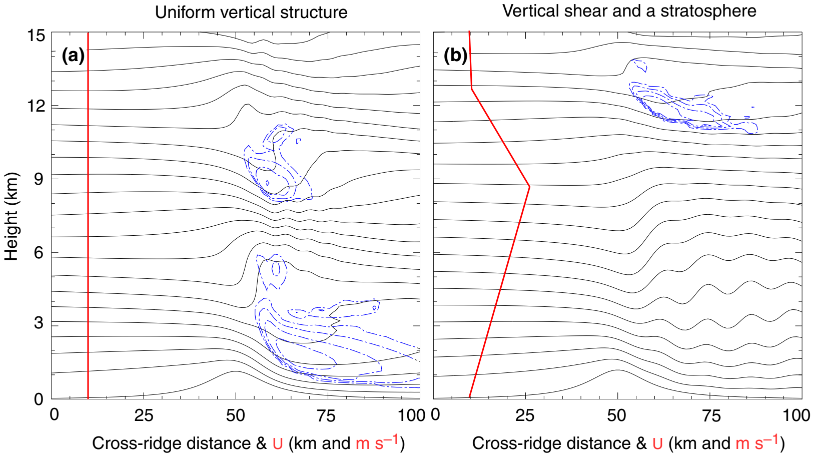

Figure 6 Streamlines (black), contours of the subgrid-scale eddy diffusivity (blue dot-dashed, at intervals of 20 m^2 s^{-1}) and the vertical profile of the large-scale wind (red) for (a) the case shown in **Figure 3(a)** except that $Nh_0/U = 1.2$ and the vertical scale extends to 15 km; (b) as in (a) except with westerly wind shear throughout the tropopause and a realistic stratosphere (see text).

most real-world wave-breaking events, in which the wave structure is significantly modified by vertical wind shear in the upstream flow. Those ridges that run north–south in the middle latitudes are oriented perpendicular to the climatological westerly flow and are frequent generators of large-amplitude mountain waves. A prototypical example of the mountain waves generated by such ridges in a deep westerly flow is shown in **Figure 6(b)**. The mountain profile, the surface wind speed (10 m s^{-1}), and the low-level stability (0.01047 s^{-1}) are identical to those for the case in **Figure 6(a)**, but the upstream wind speed U increases linearly to 25 m s^{-1} at a height of 9 km. The presence of a stratosphere is modeled by increasing N to 0.02 s^{-1} above 9 km and linearly decreasing U back to 10 m s^{-1} at $z = 13$ km. The wind speed is a constant 10 m s^{-1} above 13 km. The increase in the cross-mountain wind with height throughout the troposphere decreases the local value of the nonlinearity parameter $\varepsilon(z) = N(z)h_0/U(z)$ to a minimum just below the tropopause at $z = 9$ km. Above the tropopause ε increases rapidly with height due to the factor-of-two increase in N and the reversal of the wind shear. As evident in **Figure 6(b)**, these more realistic vertical variations in the upstream flow are sufficient to shift the primary region of wave breaking to the lower stratosphere (around $z = 12$ km) and to prevent wave breaking in the troposphere.

The influence of wave breaking is highly nonlocal. In the case with constant N and U, the entire lee-side flow in the wave-breaking regime (**Figure 6(a)**) is dramatically different from that in the nonbreaking regime (**Figure 5(a)**). In particular, the surface winds above the lee slope are significantly enhanced in the wave-breaking regime (*see* **Mountain Meteorology:** Downslope Winds). The breaking waves in **Figure 6(b)** also exert a nontrivial influence on the low-level flow, although this influence is considerably less dramatic than that which develops as a consequence of wave breaking in **Figure 6(a)**.

Vertical Momentum Transport

When air flowing over a mountain generates vertically propagating waves, a region of high pressure develops upstream of the ridge crest and a region of low pressure appears in the lee. The distribution of these pressure perturbations is revealed by the along-flow variation in the spacing between the two lowest streamlines in Figures 3(b), 4(a), 5 and 6. The asymmetry in the pressure distribution across the ridge gives rise to a net pressure force on the topography that tends to accelerate the topography in the direction of the mean flow. An equal and opposite force is exerted on the mean flow by the topography.

To see how the topographically induced decelerative forcing is distributed throughout the fluid, consider the horizontal momentum eqn [17] in which $\mathbf{v}$ is the total velocity vector, p is the pressure, ρ is the density, $\mathbf{i}$ is the unit-vector along the x-coordinate, and $u = \mathbf{v}\cdot\mathbf{i}$,

$$\frac{\partial \rho u}{\partial t} + \nabla\cdot(\rho u\mathbf{v} + p\mathbf{i}) = 0. \qquad [17]$$

Integrate the preceding throughout the volume between the surface $h(x)$ and an arbitrary level z_t; use the divergence theorem; note that there is no advective momentum flux through the lower boundary, and assume that the domain is periodic in the horizontal, then

$$\frac{\partial}{\partial t}\iiint \rho u\,\mathrm{d}V = -\iint \rho u w\,\mathrm{d}x\mathrm{d}y\bigg|_{z=z_t} - \iint p\frac{\partial h}{\partial x}\,\mathrm{d}x\mathrm{d}y\bigg|_{z=h}. \qquad [18]$$

When vertically propagating mountain waves are present, the cross-mountain pressure drag (given by the last term in eqn [18]) must decelerate the volume-averaged flow in the layer between the surface and z_t unless that drag is balanced by a downward transfer of momentum through level z_t. This same result can be obtained for flow in nonperiodic domains under the assumption that the perturbation quantities vanish at the lateral boundaries, although caution is advised when trying to apply eqn [18] in a nonperiodic domain because non-negligible mountain-wave-induced perturbations may extend far upstream and downstream from a very long ridge.

The interaction between the mean flow and the mountain-wave induced momentum fluxes can be described more precisely by separating the dynamical variables into an average over the domain (denoted by an overbar and taken as the representative of the synoptic-scale flow impinging on the mountain) and the perturbation about that average (denoted by a prime and assumed to represent the contributions from mountain waves generated by the flow over the ridge). If the horizontal momentum equation for two-dimensional inviscid Boussinesq flow,

$$\frac{\partial \rho_0 u}{\partial t} + \frac{\partial}{\partial x}\left(\rho_0 u^2 + p\right) + \frac{\partial}{\partial z}\left(\rho_0 u w\right) = 0, \qquad [19]$$

is averaged over a periodic domain (or if it is assumed that the perturbations vanish at the lateral boundaries of a nonperiodic domain) and if $\overline{w} = 0$, one obtains

$$\frac{\partial \rho_0 \overline{u}}{\partial t} = -\frac{\partial}{\partial z}\left(\rho_0 \overline{u'w'}\right). \qquad [20]$$

A decelerative forcing will therefore be exerted on the flow in those regions in which the mountain-wave-induced momentum flux is divergent, that is, where $\partial\left(\rho_0 \overline{u'w'}\right)/\partial z > 0$.

The vertical profile of the momentum flux is particularly easy to describe for steady, inviscid, small-amplitude waves in a periodic domain (or in an unbounded domain in which the waves decay as $x \to \pm\infty$). The cross-mountain pressure drag in such waves is identical to the vertical momentum flux at $z = 0$, as may been seen from the steady-state version of eqn [18] in the limit $z_t \to 0$. Furthermore, a classic theorem due to Eliassen and Palm states that under the preceding assumptions $\rho_0 \overline{u'w'}$ is constant with height except at a 'critical level' at which $\overline{u} = 0$. Mountain waves are dissipated at the mean-state critical layers found in real atmospheric flows. Mountain waves are also dissipated through breaking and overturning if they attain sufficiently large amplitude due to the decrease in density with height or, as in **Figure 6**, if they propagate into a region in which the local value of N/U increases significantly. Small-amplitude mountain waves that propagate all the way to the mesosphere without experiencing overturning are damped by radiative heat transfer.

The Eliassen and Palm theorem implies that small-amplitude mountain waves transport a fraction of the momentum of the cross-mountain flow downward to the surface from those elevations at which the waves undergo dissipation. There will be no vertical momentum flux divergence and no forcing of the mean flow within the those layers of the atmosphere in which the waves are steady and nondissipative. The momentum fluxed downward by the waves is transferred to the topography by the cross-mountain pressure drag. Similar distributions of the vertical momentum flux are obtained even when the waves are nonlinear. For example, the vertical momentum flux profile associated with the finite-amplitude waves shown in **Figure 6(b)** is approximately nondivergent between the ground and the region of wave breaking in the layer $11 \le z \le 13$ km. In contrast, the momentum flux profile is strongly divergent in the wave breaking region, and the mean flow is subject to a significant decelerative forcing throughout this layer (*see* **Dynamical Meteorology:** Wave Mean-Flow Interaction). Unlike surface friction, the drag associated with mountain waves is typically exerted on the flow well above the lower boundary. Numerical experiments with general circulation models suggest that mountain-wave-induced drag plays a nontrivial role in the total momentum budget of the atmosphere.

Nonsteady Waves

The assumption that mountain waves are in steady state greatly simplifies their theoretical analysis and leads to predictions that are often in decent agreement with observations. Nevertheless, clear evidence of nonstationary behavior has also been documented, particularly in the case of trapped lee waves. Trapped waves are resonant oscillations whose amplitude and wavelength are quite sensitive to changes in the structure of the flow impinging on the mountain. Thus, rather modest changes in the large-scale wind speed and temperature profiles can produce easily observed variations in the lee wave train. Even when the large-scale synoptic forcing is essentially constant, lee-wave transience can be produced by either nonlinear wave–wave interactions or by the diurnal heating or cooling of the planetary boundary layer. Solar heating, for example, reduces the buoyancy frequency $N(z)$ in the lower atmosphere in a manner that typically tends to increase the wavelengths of trapped waves.

Although it can be more difficult to observe, changes in the large-scale flow also influence vertically propagating waves. One property of vertically propagating waves that is particularly sensitive to variations in the cross-mountain flow is the vertical profile of momentum flux. An example of this sensitivity is shown in **Figure 7**, which is a plot of $\rho_0 \overline{u'w'}$ as a function of time and height from a numerical simulation in which a localized jet crosses over an isolated ridge.

The large-scale winds are constant with height, and over the ridge crest they increase sinusoidally from zero to 20 m s^{-1} and then fall back to zero over a 50-h period. Throughout the domain $N = 0.01$ s^{-1}, so at specific times during the simulation, the flow in a vertical plane perpendicular to the ridge-line

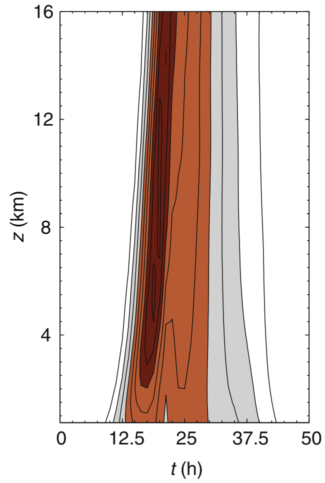

Figure 7 Horizontal-domain-averaged momentum flux $\rho_0 \overline{u'w'}$ generated by time-varying flow over a 750-m high ridge plotted as a function of time and height. Values are normalized by the momentum flux for the linear steady-state solution for waves driven by a 20 m s^{-1} flow across the same ridge. Solid lines show contours at intervals of 0.25, with values in the range (0.5,1.0), (1.0,1.75), and greater than 1.75 shaded gray, orange, and dark orange-red, respectively. Adapted with permission from Chen, C.C., Durran, D.R., Hakim, G.J., 2005. Mountain wave momentum flux in an evolving synoptic-scale flow. Journal of Atmospheric Sciences 62, 3213–3231.

is roughly similar to that shown in Figures 5(a) and 6(a), except that the ridge in the simulation used to produce Figure 7 is 750 m high. The actual momentum flux is normalized by the flux produced by linear waves over a mountain of the same height and shape in a steady uniform 20 m s^{-1} flow (with the same value of $N = 0.01$ s^{-1}). As a point of reference, if nonlinear processes were negligible, and if the 50-h period over which the flow varies were sufficiently long that the waves could be considered steady, the Eliassen-Palm theorem would apply, in which case every contour drawn in Figure 7 would be a straight vertical line and the contours would be symmetric about hour 25 because the momentum flux would be linearly proportional to the wind speed. Because of the normalization, the contour at hour 25 would have a value of unity, and there would be no orange region on the plot.

Yet as apparent in Figure 7, the momentum fluxes are not symmetric about hour 25, but are much stronger when the large-scale flow is accelerating ($t < 25$ h) than when it is decelerating ($t > 25$ h). For example, the momentum flux is three times stronger at hour 19 than at hour 31, even though the large-scale wind above the ridge at both times is identical. Moreover, the flux aloft at hour 19 is more than twice as strong as the flux that would be predicted to occur at the time of strongest flow using a steady-state analysis. This momentum-flux enhancement may be explained by noting that each packet of wave energy launched while the mountain wave is present moves upward at the group velocity. In this example, the vertical group velocity of each packet is proportional to the large-scale cross-mountain wind speed at the time the packet was launched. As a consequence, packets launched later in the acceleration phase tend to overtake those launched earlier and accumulate above the mountain, creating higher momentum fluxes while the cross-mountain flow is accelerating.

The drag generated by the vertical divergence of mountain-wave generated momentum fluxes is currently parameterized in global atmospheric models for both weather forecasting and climate simulation. The formulation of accurate 'gravity-wave-drag' parameterizations is greatly complicated both by the nonlinearity of finite-amplitude mountain waves in (compare Figures 4(b) and 5(b)) and by the dependence of the flux on the past history of the large-scale flow.

See also: **Dynamical Meteorology:** Wave Mean-Flow Interaction. **Gravity Waves:** Buoyancy and Buoyancy Waves: Optical Observations; Buoyancy and Buoyancy Waves: Theory. **Mountain Meteorology:** Downslope Winds; Lee Vortices.

Further Reading

Baines, P.G., 1995. Topographic Effects in Stratified Flows. Cambridge University Press, Cambridge.

Chen, Chih-Chieh, Durran, Dale R., Hakim, Gregory J., 2005. Mountain wave momentum flux in an evolving synoptic-scale flow. Journal of Atmospheric Sciences 62, 3213–3231.

Durran, D.R., 1986. Mountain waves. In: Ray, Peter S. (Ed.), Mesoscale Meteorology and Forecasting. American Meteorological Society, Boston, pp. 472–492.

Eliassen, A., Palm, E., 1960. On the Transfer of Energy in Stationary Mountain Waves, vol. 22. Geof. Publikasjoner, pp. 1–23.

Gill, Adrian E., 1982. Atmosphere–Ocean Dynamics. Academic Press, Orlando, p. 662.

Holton, James R., 1992. An Introduction to Dynamic Meteorology, third ed. Academic Press, San Diego. p. 507.

Smith, R.B., 1979. The influence of the mountains on the atmosphere. In: Saltzman, B. (Ed.), Advances in Geophysics, vol. 21. Academic Press, pp. 87–230.

Encyclopedia of Atmospheric Sciences, Second Edition, 2015, 95–102